provided the author and source are cited.

Structural Evolution and Atom Clustering in β-SiAlON: β-Si$_{6-z}$Al$_z$O$_z$N$_{8-z}$

Clayton Cozzan,[†,‡,§] Kent J. Griffith,[⊥] Geneva Laurita,[†,§] Jerry G. Hu,[§] Clare P. Grey,*[⊥] and Ram Seshadri*[†,‡,§,‖]

[†]Mitsubishi Chemical Center for Advanced Materials, [‡]Materials Department, [§]Materials Research Laboratory, and [‖]Department of Chemistry and Biochemistry, University of California, Santa Barbara, California 93106, United States

[⊥]Department of Chemistry, University of Cambridge, Lensfield Road, Cambridge CB2 1EW, United Kingdom

S Supporting Information

ABSTRACT: SiAlON ceramics, solid solutions based on the Si$_3$N$_4$ structure, are important, lightweight structural materials with intrinsically high strength, high hardness, and high thermal and chemical stability. Described by the chemical formula β-Si$_{6-z}$Al$_z$O$_z$N$_{8-z}$, from a compositional viewpoint, these materials can be regarded as solid solutions between Si$_3$N$_4$ and Al$_3$O$_3$N. A key aspect of the structural evolution with increasing Al and O (z in the formula) is to understand how these elements are distributed on the β-Si$_3$N$_4$ framework. The average and local structural evolution of highly phase-pure samples of β-Si$_{6-z}$Al$_z$O$_z$N$_{8-z}$ with z = 0.050, 0.075, and 0.125 are studied here, using a combination of X-ray diffraction, NMR studies, and density functional theory calculations.

β–Si$_{6-z}$Al$_z$O$_z$N$_{8-z}$

$\mathcal{H}\phi_i(\mathbf{r}) = \epsilon_i\phi_i(\mathbf{r})$

^{27}Al NMR, δ (ppm)

AlON$_3$

Synchrotron X-ray diffraction establishes sample purity and indicates subtle changes in the average structure with increasing Al content in these compounds. Solid-state magic-angle-spinning ^{27}Al NMR experiments, coupled with detailed ab initio calculations of NMR spectra of Al in different AlO$_q$N$_{4-q}$ tetrahedra ($0 \leq q \leq 4$), reveal a tendency of Al and O to cluster in these materials. Independently, the calculations suggest an energetic preference for Al−O bond formation, instead of a random distribution, in the β-SiAlON system.
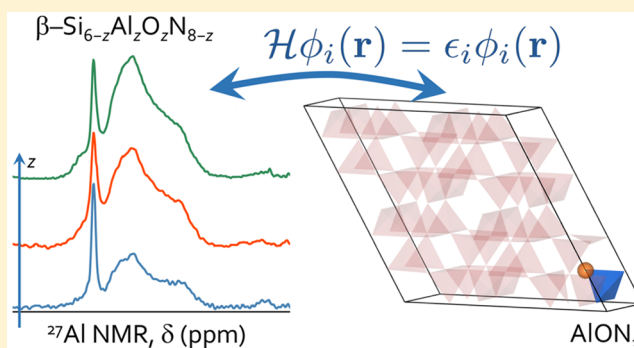
INTRODUCTION

SiAlON ceramics can be regarded as solid solutions between the compositions Si$_3$N$_4$ and Al$_3$O$_3$N. These ceramics are useful for their excellent mechanical properties, such as high hardness, high strength, wear resistance, and resistance to thermal shock.[1] In these systems, Al is substituted for Si and, concomitantly, O for N. In SiAlONs, anion ordering is driven by differences in the bonding, size, and charge, and the resulting clustering can have large effects on the behavior of optical SiAlONs.[2] To understand anion ordering in SiAlONs, local structural techniques must be utilized. X-ray diffraction is not sufficient because the scattering factors of both Si and Al and also O and N are too similar, preventing precise occupancy information from being obtained. Extended X-ray absorption fine structure (EXAFS) suffers the same issues of contrast and is difficult to implement when substituent concentrations are low. The neutron pair distribution function technique could cast light on the problem, but once again, this technique would be limited in utility and scope at the low concentrations of Al and O considered here. Solid-state magic-angle-spinning (MAS) NMR of ^{27}Al offers a potential solution, providing insight into the local coordination environment of the Al nucleus.

Early structural investigation of Si$_{6-z}$Al$_z$O$_z$N$_{8-z}$ using MAS NMR observed that ^{27}Al is a nucleus sensitive to coordination and geometry, whereas ^{29}Si is not, with spectra showing Si tetrahedrally coordinated in a SiAlON that does not change with increased Al and O substitution.[3,4] Investigations of SiAlONs using MAS ^{27}Al NMR revealed that, rather than a random distribution of Si and Al on metal sites and O and N on nonmetal sites or a preference for Al−N and Si−O bonds, there is a preference for Al−O and Si−N bonds.[4−6] This preference has also been verified using Monte Carlo simulations and neutron diffraction on other SiAlON systems.[7] Most early NMR studies suggested the existence of mixed tetrahedra,[8] which was supported by EXAFS showing a decrease of the average bond length for the first coordination sphere of Si with increasing Al and O.[4]

Broadening is observed in MAS ^{27}Al NMR spectra and associated with distorted tetrahedra from a range of AlO$_q$N$_{4-q}$ ($0 \leq q \leq 4$). It was proposed that the distribution changes with decreasing Al because more of the mixed AlO$_3$N and AlO$_2$N$_2$ are present, which are broader, and the AlN$_4$ peak intensity decreases with increasing Al because of AlO$_3$N and AlO$_2$N$_2$ formation.[6] As the composition of SiAlON approaches AlN, the proportion of AlN$_4$ tetrahedra relative to AlON$_3$ tetrahedra

increases.[8,9] Conversely, in the formula $Si_{3-z}Al_zO_zN_{4-z}$ for $z \approx$ 0.5−1, it was observed that substitutional O is strictly coupled to $Al(O,N)_4$ tetrahedra with a range of tetrahedral coordinations.[5] These early NMR works observed changes in line shape as a function of the Al−O content but could not resolve them into distinct coordination environments because of the moderate fields used. More recently, work using X-ray absorption near-edge spectroscopy and computation showed evidence for Al−O bonds in SiAlON, with the pairing of Al and O having an energy benefit of a few tenths of an electronvolt per Al−O pair.[10]

Here, samples of β-$Si_{6-z}Al_zO_zN_{8-z}$ systematically varying Al content ($z = 0.050$, $z = 0.075$, and $z = 0.125$) are studied. Synchrotron X-ray diffraction was utilized to investigate the average structure changes in this system as a function of systematic variation in the Al content. Synchrotron X-ray diffraction and prior neutron scattering work on the same samples (to establish composition) confirm phase purity and demonstrate that the actual composition is the nominal composition.[11] Ab initio periodic density functional theory (DFT)-based calculations of NMR parameters and structural energetics, along with high-field MAS ^{27}Al NMR measurements, were employed to elucidate local structure details of the Al site in the SiAlON structure. Improvements in the NMR hardware, coupled with quantum-chemical calculations, have enabled the identification and quantification of Al coordination environments. Simulations of quadrupolar NMR line shapes highlight the inherent inability of previous moderate field studies to resolve any but the highly symmetric AlO_4/AlN_4 sites. Clustering of Al and O in the SiAlON structure is observed experimentally and supported independently by DFT enthalpies and a comparison of the calculated Al environments to experimental spectra collected in the current work. The current work is therefore the first high-field NMR study of completely phase-pure β-$Si_{6-z}Al_zO_zN_{8-z}$ and is also the first time DFT calculations have been employed to assign spectra and determine energetics in these systems.

Besides helping to understand the distribution of Al and O in the β-SiAlON phases, the present work points to the general utility of employing high-resolution, high-field NMR techniques, in the appropriate combination with DFT calculations, to unravel the intricate details of local compositional variation in functional materials. Studies such as these could profit a variety of functional material classes where small amounts of dopants are known to have important effects. These include zeolites,[12] phosphors,[11,13] diluted magnetic semiconductors,[14] and thermoelectric materials.[15]

■ METHODS

To obtain accurate control over the concentration of Al^{3+} and O^{2-}, a high-pressure and high-temperature synthesis route was used. Powders of α-Si_3N_4 and Al_2O_3 were ground with nominal stoichiometry $Si_{6-z}Al_zO_zN_{8-z}$ in an alumina pestle. The powders were heated in a boron nitride crucible at 1950 °C for 12 h under $N_2(g)$ (>99.9995%) at a pressure of 0.92 MPa and annealed in argon for 8 h before being ground into a fine powder and washed using a mixture of HNO_3 and HF.

Synchrotron powder X-ray diffraction was performed at room temperature at the 11-BM beamline at the Advanced Photon Source, Argonne National Laboratory. The calibrated wavelength was $\lambda = 0.459001$ Å for $z = 0.075$ and $\lambda = 0.413194$ Å for $z = 0.050$ and 0.125. Rietveld refinements were performed using the General Structure Analysis System (GSAS) with EXPGUI.[16,17] Peak shapes were handled using the pseudo-Voigt profile function, which combines Gaussian and Lorentzian components. The background was handled using a Chebyshev polynomial. The occupancies were left as nominal because of the lack of contrast of scattering between Al and Si and between O and N. The refined structures were visualized using the open-source crystallographic software VESTA.[18]

Solid-state ^{27}Al NMR was conducted at room temperature using a Bruker AVANCE III Ultrashield Plus 800 MHz (18.8 T) narrow-bore (54 mm) spectrometer with a 3.2 mm Tri-Gamma HXY triple-resonance MAS probe with a transmitter frequency of 208.52 MHz for the 100% naturally abundant ^{27}Al nuclei. Samples were packed into a 3.2 mm zirconia rotor (Bruker) and spun at 20 kHz for 24 h of data collection due to the low Al content. The radio-frequency (RF) pulse length (3.6 μs) and power (117.5 W) were chosen to achieve a 15° pulse ($\pi/12$) rotation of the net ^{27}Al magnetization for quantitative measurements. Shifts were referenced to 1 M $Al(NO_3)_3$(aq) at 0 ppm. The resonance frequency for nuclei with nonzero nuclear quadrupolar coupling constants (NQCCs; C_Q) is influenced by electronic shielding as well as a quadrupolar term; thus, it is correct to refer to shifts, rather than chemical shifts, for quadrupolar nuclei such as ^{27}Al. Data treatment was performed using the SOLA interface in *Topspin 3.2*. Simulations were performed on the central ($+^1/_2 \leftrightarrow -^1/_2$) and satellite transitions ($\pm^1/_2 \leftrightarrow ^3/_2$ and $\pm^3/_2 \leftrightarrow ^5/_2$) with second-order perturbation theory treatment of the quadrupolar interaction. Ab initio DFT calculations of the enthalpy and NMR parameters were performed in the CASTEP plane-wave code.[19−22] The Perdew−Burke−Ernzerhof[23] exchange-correlation functional, a generalized gradient approximation functional, was employed. Core electrons were approximated with Vanderbilt "ultrasoft" pseudopotentials generated "on-the-fly" in CASTEP 8.0. The SiAlON system required a basis set of plane waves with energies up to 600 eV and a Monkhorst−Pack[24] grid corresponding to a Brillouin zone sampling finer than $2\pi \times 0.05$ Å^{-1}. Convergence with respect to the basis set energy and Brillouin zone sampling was confirmed. Under these conditions, enthalpy, σ_{iso}, and C_Q were converged to within 0.1 eV, 0.1 ppm, and 0.1 MHz, respectively. The reference equation used to convert shielding to shift was determined via linear regression from a series of Al compounds and is detailed in the Supporting Information. Numerical simulations of the quadrupolar NMR line shapes were performed from the ab initio ^{27}Al NMR tensors in the SIMPSON[25] program at 18.8 T and 20 kHz MAS to compare with the spectra collected in this study. The effect of the unit cell size in the calculations was evaluated by comparing calculations with the lattice parameters fixed at the values determined from synchrotron diffraction for $z = 0.050$, 0.075, and 0.125 as well as when the cell was allowed to relax from the initial values for $z = 0.075$.

■ RESULTS AND DISCUSSION

β-$Si_{6-z}Al_zO_zN_{8-z}$ consists of densely packed, corner-sharing $(Si,Al)(O,N)_4$ tetrahedra with ABAB stacking[5] and crystallizes in the hexagonal space group $P6_3$ (No. 173) with a channel along the c axis.[11,26,27] Rietveld refinements of synchrotron X-ray data indicate phase purity in the β-SiAlON samples. Figure 1 shows the room temperature fit and refined structure for $z = 0.075$, with detailed structural refinements of atomic positions and refined atomic displacement parameters (U_{iso}) for all samples shown in Table 1.

Small atomic displacement parameters are linked to high structural rigidity.[11,28] In the present work, the thermal displacement parameters are small, and therefore the rigidity does not change much with small substitution levels. It can be seen that the U_{iso} values for $z = 0.075$ are the lowest, but because the X-ray scattering factors of O and N are too similar, there are not significant differences in any of the U_{iso} values that dictate a clear trend, and the differences are in some cases within the standard deviation of the refinement. In general, all samples have small atomic displacement parameters, which indicates that the rigidity of the structure is not reduced at small
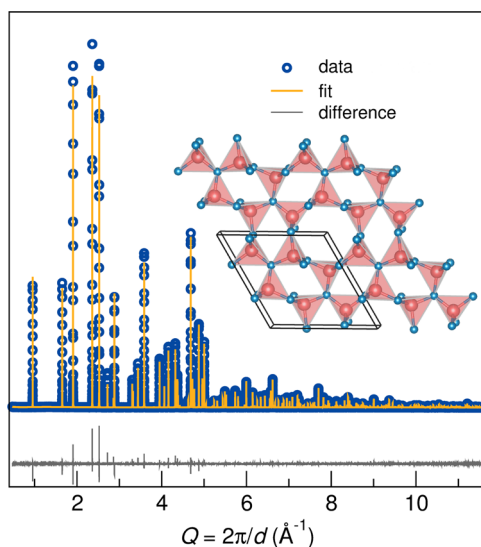
Figure 1. Synchrotron X-ray diffraction data (blue circles), refinement (fit, orange), difference between the data and fit (gray line), and refined structure (inset) for β-Si$_{6-z}$Al$_z$O$_z$N$_{8-z}$ with $z = 0.075$.


Figure 2. (a) Unit cell edges and (b) volume as a function of z determined through synchrotron X-ray diffraction show an increase in all parameters with z. Error bars are contained within the data points.

Table 1. Structural Data Obtained from Rietveld Refinements of Synchrotron X-ray Diffraction Data for β-Si$_{6-z}$Al$_z$O$_z$N$_{8-z}$ with $z = 0.075$[a]

	Al content (z)		
	0.050	0.075	0.125
cell a (Å)	7.60584(1)	7.60692(2)	7.60853(2)
cell c (Å)	2.908444(7)	2.909039(7)	2.910116(7)
cell V (Å^3)	145.7090(4)	145.7800(5)	145.8960(5)
Si/Al x	0.7685(5)	0.7685(4)	0.7685(2)
Si/Al y	0.1747(5)	0.1747(4)	0.1744(2)
Si/Al z	0.291(5)	0.250(3)	0.290(5)
O1/N1 x	0.0298(4)	0.0296(3)	0.0296(4)
O1/N1 y	0.3292(4)	0.3298(3)	0.3296(5)
O1/N1 z	0.303(4)	0.2670(3)	0.6975(4)
O2/N2 z	0.281(7)	0.238(6)	0.28(5)
Si/Al U_{iso} (Å^2)	0.0030(2)	0.0022(5)	0.0035(2)
O1/N1 U_{iso} (Å^2)	0.0031(4)	0.0023(4)	0.0039(6)
O2/N2 U_{iso} (Å^2)	0.0026(9)	0.0006(8)	0.0022(5)

[a]The numbers in parentheses show standard deviations on the last number. O1 and N1 are located on the 6c Wyckoff site in the unit cell, and O2 and N2 are located on the 2b Wyckoff site in the unit cell.

Al substitution levels. Also observed with increasing Al content is the increase in the unit cell parameters in both the a and c direction, which leads to an overall increase in the unit cell volume.[5] An ionic radii argument can explain this expansion because Al^{3+} has a larger radius than Si^{4+} (0.39 and 0.26 Å for the coordination number CN = 4, respectively).[29] This also involves incorporating O^{2-} to charge balance, which is smaller than N and therefore would compete with the expansion.

Lattice parameters shown in Table 1 highlight the increase in the unit cell volume with increasing Al content (visualized in Figure 2a). While an increase in the unit cell volume does not guarantee an increase in these bond distances, the average bond length around this site increases from 2.6698 Å in $z = 0.050$ to 2.6877 Å in $z = 0.125$.

Si$_3$N$_4$ crystallizes in a unit cell with six Si atoms and eight N atoms ($z = 2$). For ab initio calculations, in order to study representative Al and O substitution levels, $2 \times 2 \times 2$ (48 Si/64
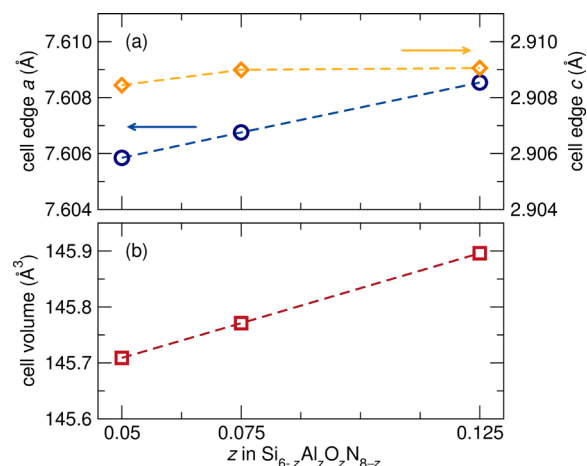
N, example defect structures shown in Figure 3) and $2 \times 2 \times 4$ (96 Si/128 N) supercells were created with Al−O pairs swapped into the new cells, representing from $z = 0.0625$ for one Al−O pair in the latter supercell to $z = 1$ for eight Al−O pairs in the former supercell in Si$_{6-z}$Al$_z$O$_z$N$_{8-z}$. For calculations of the defect energetics, the unit cell parameters were fixed to the experimental values found in this study for the intermediate Al content ($z = 0.075$) and atomic coordinates relaxed to local minima with DFT forces. Bond lengths obtained from diffraction and DFT show that, for Si$_3$N$_4$, the Si−N bond lengths range from 1.70 to 1.77 Å. In low-Al SiAlONs, the Si−N bond lengths show a very slight contraction, with bond lengths ranging from 1.68 to 1.76 Å. Si−O (1.74−1.77 Å), Al−N (1.77−1.83 Å), and Al−O (1.82−1.88 Å) bond ranges obtained from DFT confirm that Al forms longer bonds than Si and O forms longer bonds than N, all of which supports the observation of unit cell expansion with increasing z obtained from Rietveld refinements of the diffraction data.

NMR calculations for magnetic shielding, shielding anisotropy, and the electric field gradient (EFG) tensor were performed. The ^{27}Al C_Q ranges (MHz) versus $\delta(^{27}$Al) (ppm) ranges computed in this study are shown in Figure 4. The fits of the experimental NMR data are shown in Figure 5, with the parameters shown in Table 2. Line shapes were fit to the data as informed by the range of values for each parameter from the calculations. Only the central line of the experimental spectra was fit. The relatively low intensity of the spinning side bands as well as baseline distortions, both common issues for small quantities of quadrupolar nuclei, would complicate inclusion of the spinning side-band manifold. Pseudo-Voigt broadening was applied. As the calculations indicate, the NMR parameters are dominated by nearest neighbors but are still significantly affected by next-nearest neighbors and beyond. While to the first coordination shell (one bond, <2.25 Å) there are only five possible local environments for Al (i.e., AlO$_q$N$_{4-q}$ where $0 \leq q \leq 4$), the number of distinct environments increases rapidly with the cluster size. For simplicity, the smallest number of possible sites was used to achieve a satisfactory fit, but it is likely that there are many similar Al sites. C_Q values of 0 were not observed computationally or experimentally for the AlO$_4$ or AlN$_4$ sites, which is due to the fact that the tetrahedra are distorted, even in the Si$_3$N$_4$ structure with no site disorder (via DFT, the EFG tensor is nonzero at the Si nucleus in Si$_3$N$_4$ but
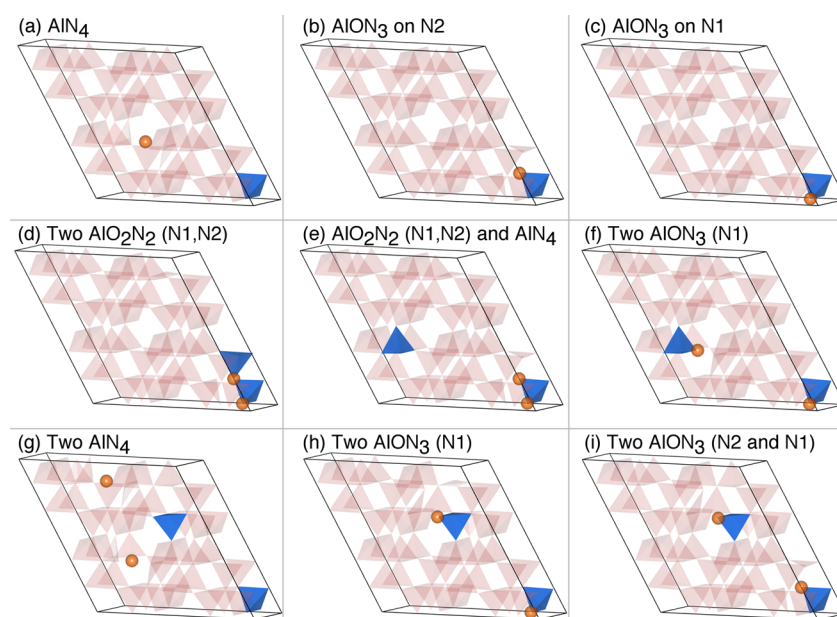
Figure 3. Defect structures for $2 \times 2 \times 2$ supercells with composition $Si_{48-x}Al_xN_{64-x}O_x$, where $x =$ (a−c) 1 and (d−i) 2. Si−N tetrahedra are red, Al tetrahedra are blue, and O atoms are orange and exaggerated in size for visibility. The defects follow the order of Table 3 and correspond to (a) AlN_4, (b) $AlON_3$ on the N2 site, (c) $AlON_3$ on the N1 site, (d) AlO_2N_2 (N1 and N2) and AlO_2N_2 (N1 and N2), (e) AlO_2N_2 (N1 and N2) and AlN_4, (f) $AlON_3$ (N1) and $AlON_3$ (N1), (g) AlN_4 and AlN_4, (h) $AlON_3$ (N1) and $AlON_3$ (N1), and (i) $AlON_3$ (N2) and $AlON_3$ (N1). The anions O1 and N1 are located on the 6c Wyckoff site, and O2 and N2 are located on the 2b Wyckoff site in the supercell.
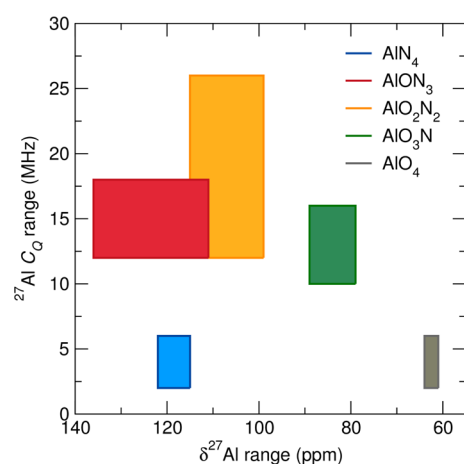
Figure 4. Calculated ranges for ^{27}Al C_Q (MHz) and δ (ppm) for various tetrahedral environments.

Si is an $I = {}^1/_2$ nucleus, meaning that it cannot be observed experimentally). While the other environments could be axially symmetric with an η value close to 1, this is also not observed. The symmetry is further broken by the presence of long-range defects away from the AlO_4 or AlN_4 sites. In addition, simulations of quadrupolar NMR line shapes for different fields and spinning rates (Supporting Information) highlight the requirement for ultrahigh field and high spinning speeds to resolve the Al sites in SiAlONs. These data should prove useful for planning and executing future NMR studies of this large family of materials.

Further evidence for the experimentally observed preference for $AlON_3$ formation and its subsequent effects on the population of other tetrahedral environments is observed by comparing the experiment to a statistical model and is shown in Figure 6. From the DFT-informed fits of the experimental NMR data, the ratio of AlN_4−$AlON_3$−AlO_2N_2/AlO_3N is
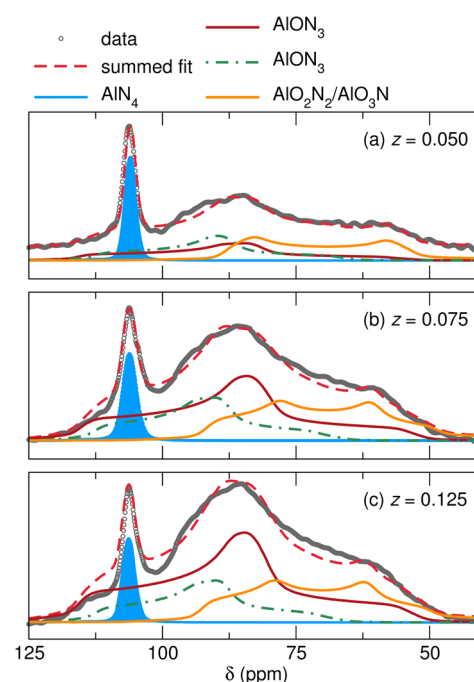

Figure 5. ^{27}Al NMR spectra at 18.8 T and 20 kHz MAS for $z =$ (a) 0.050, (b) 0.075, and (c) 0.125 demonstrating the increase in the contribution from $AlON_3$ as a function of increasing Al. The experimental data (gray circles) are overlaid by the summed fit (red dashed line), which is comprised of an AlN_4 defect (blue line), two different $AlON_3$ environments (maroon and light-green lines), and AlO_2N_2/AlO_3N (orange line). For clarity, in part (a), fit contributions are separated from the data.

16:54:30 for $z = 0.050$, 8:64:28 for $z = 0.075$, and 7:69:24 for $z = 0.125$, with an approximate error estimate of 5% due to site overlap. The relative intensities were fit by least-squares refinement with the DFT-calculated values used as initial

Table 2. NMR Parameters for Fits from Figure 5 as Informed by DFT Calculations[a]

	site			
	AlN_4	$AlON_3$	$AlON_3$	$AlO_2N_2/$ AlO_3N
$\delta\,^{27}Al$ shift (ppm)	108(1)	113(5)	116(5)	96(5)
C_Q (MHz)	3.4(0.5)	11.0(0.5)	12.8(0.5)	13.2(0.5)
η_Q	0.50(0.10)	0.80(0.10)	0.90(0.10)	0.40(0.10)

[a]The numbers in parentheses show uncertainties.
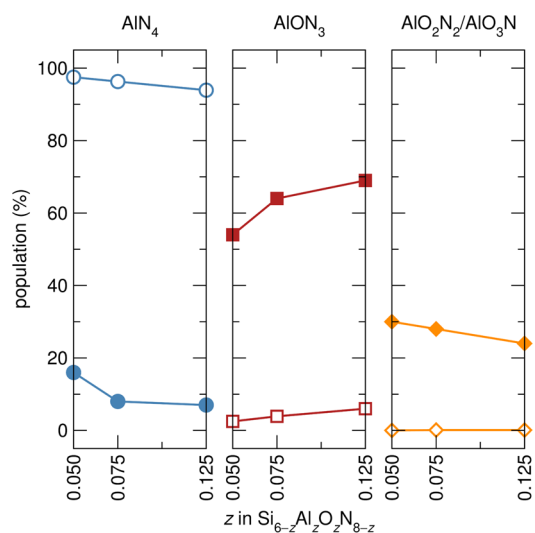
Figure 6. Populations obtained from fitting the experimental NMR data (closed shapes) showing a definite preference for $AlON_3$ formation and a decrease in the AlN_4 and AlO_2N_2/AlO_3N populations. This is in stark contrast to the stochastic model (open shapes), which predicts a high population of AlN_4 environments, a low population of $AlON_3$ tetrahedra, and virtually no AlO_2N_2/AlO_3N.

values. A stochastic model (Supporting Information) (i.e., random, statistical distribution) predicts 97.5%, 96.3%, and 93.9% AlN_4 for samples 0.050, 0.075, and z =0.125, respectively, providing further evidence for preferential Al−O bond formation instead of a random distribution of Al and O within the Si_3N_4 structure. For $AlON_3$, the stochastic model predicts 2.5%, 3.6%, and 6.0% for z = 0.050, 0.075, and 0.125, respectively, and virtually zero (0.0%, 0.1%, and 0.1%) for AlO_2N_2. Thus, there is a definite preference for $AlON_3$ formation experimentally.

DFT calculations of the energies for various tetrahedral environments (Figure 3) performed on a 2 × 2 × 2 supercell with relaxed atomic coordinates and with z = 0.075 lattice parameters are provided in Table 3 referenced to the least favorable configuration. Variation of the lattice parameters in the range determined from synchrotron diffraction yielded defect enthalpies within ±0.04 eV of the intermediate lattice parameters used for enthalpy calculations. Thus, the increase in the unit cell size that accompanies the increased defect concentration does not significantly affect these calculations. In all defect configurations, the energy decreased as the number of Al−O bonds increased. For each composition, the baseline energy was calculated as the relaxed energy with Al only in AlN_4 tetrahedra and the corresponding number of O as OSi_3 (Figure 3a). For a single defect pair (Al1−O1) in the 2 × 2 × 2 supercell (corresponding to z = 0.125), the localization of Al−

Table 3. Table of Energy Values for Defects Showing an Energetic Preference for $AlON_3$ Bonding in the Two Doping Levels Closest to that Investigated Experimentally[a]

composition	defect geometry (O on N1 or N2)	eV/defect
1:1 Al−O	AlN_4	0.00
	$AlON_3$ (N1)	−1.2
	$AlON_3$ (N2)	−1.4
2:2 Al−O	AlN_4	0.00
	AlO_2N_2 (N1 and N2), AlN_4	−1.1
	$AlON_3$ (N1)	−1.2
	$AlON_3$ (N2), $AlON_3$ (N1)	−1.4
	AlO_2N_2 (N1 and N2), $AlON_3$ (N2)	−1.6

[a]A defect is defined as the introduction of one Al−O pair.

O forms a bond greater than 1 eV more stable than when the defect atoms are separated. In addition, it was discovered that O atoms prefer to sit on the N2 site (0.2−0.3 eV preference in all mixed-anion tetrahedral configurations) isolated from the large hexagonal tunnel along the c axis. Unfortunately, the two $AlON_3$ sites cannot be differentiated based on their NMR parameters, meaning the NMR data cannot be directly related to the energetics of the distinct $AlON_3$ environments. For two Al and two O, corresponding to z = 0.25, adjacent AlO_2N_2 and $AlON_3$ tetrahedra with corner-sharing Al atoms and O-corner-sharing among three tetrahedra are most energetically favorable. Defects for more than two Al and two O correspond to Al contents that are much higher than that studied experimentally in the present work (shown in Supporting Information), where the most energetically favorable tetrahedral configurations are marked by the presence of clustered defects and an increase in the number of corner-connected O atoms that are joined to two Al atoms.

Simple electrostatic bond valence sum arguments can be made to justify the stability of the Al−O pairs of the β-Si_3N_4 framework. An isolated O defect on an N site would receive three charges from neighboring Si atoms, leading it to possess a net negative charge. An isolated Al defect on an Si site would have four N neighbors, each seeking a positive charge, requiring Al to possess a net positive charge. These charge defects would annihilate and stabilize when they are nearest neighbors.

CONCLUSIONS

We have shown that Al and O have a surprising affinity for one another in the β-SiAlON structure, despite the high dilution of both Al and O in the framework. High-field solid-state ^{27}Al NMR spectral features have been assigned to different AlO_qN_{4-q} ($0 \leq q \leq 4$) species, employing DFT calculations to help in the assignment. These results suggest unambiguously that $AlON_3$ with $q = 1$ and AlO_2N_2 with $q = 2$ are found in far greater excess than would be suggested by a stochastic distribution of Al and O on the β-Si_3N_4 framework. DFT calculations of defect energetics on large supercells also suggest extra stabilization associated with Al−O clustering in the unit cell, which can be anticipated by electrostatic bond valence sum arguments. This work also shows the exquisite details of local compositional fluctuations in the crystal structure that can be unravelled by the judicious combination of high-field, high-resolution NMR experiments coupled with DFT calculations.

■ AUTHOR INFORMATION

Corresponding Authors

*E-mail: cpg27@cam.ac.uk.

*E-mail: seshadri@mrl.ucsb.edu.

ORCID Ⓞ

Kent J. Griffith: 0000-0002-8096-906X

Ram Seshadri: 0000-0001-5858-4027

Notes

The authors declare no competing financial interest.

■ REFERENCES

(1) Cao, G.; Metselaar, R. α′-Sialon ceramics: a review. *Chem. Mater.* **1991**, *3*, 242−252.

(2) Attfield, J. P. Principles and applications of anion order in solid oxynitrides. *Cryst. Growth Des.* **2013**, *13*, 4623−4629.

(3) Butler, N.; Dupree, R.; Lewis, M. H. The use of magic-angle-spinning NMR in structural studies of Si-Al-ON phases. *J. Mater. Sci. Lett.* **1984**, *3*, 469−470.

(4) Sjöberg, J.; Harris, R. K.; Apperley, D. C. ^{29}Si, ^{27}Al and ^{15}N magic-angle spinning nuclear magnetic resonance study of O′-Sialons and some related phases. *J. Mater. Chem.* **1992**, *2*, 433−438.

(5) Dupree, R.; Lewis, M.; Leng-Ward, G.; Williams, D. Co-ordination of Si atoms in silicon-oxynitrides determined by magic-angle-spinning NMR. *J. Mater. Sci. Lett.* **1985**, *4*, 393−395.

(6) Smith, M. E. Observation of mixed aluminum oxynitride (Al(O,N)$_4$) structural units by aluminum-27 magic angle spinning NMR. *J. Phys. Chem.* **1992**, *96*, 1444−1448.

(7) Vinograd, V. L.; Juarez-Arellano, E. A.; Lieb, A.; Knorr, K.; Schnick, W.; Gale, J. D.; Winkler, B. Coupled Al/Si and O/N order/

disorder in BaYb[Si$_{4−x}$Al$_x$O$_x$N$_{7−x}$] sialon: neutron powder diffraction and Monte Carlo simulations. *Z. Kristallogr.* **2007**, *222*, 402−415.

(8) Dupree, R.; Lewis, M. H.; Smith, M. Structural characterization of ceramic phases with high-resolution ^{27}Al NMR. *J. Appl. Crystallogr.* **1988**, *21*, 109−116.

(9) Klinowski, J.; Thomas, J.; Thompson, D.; Korgul, P.; Jack, K.; Fyfe, C.; Gobbi, G. Structural studies of sialon ceramics by high-resolution solid-state NMR. *Polyhedron* **1984**, *3*, 1267−1269.

(10) Tatsumi, K.; Mizoguchi, T.; Yoshioka, S.; Yamamoto, T.; Suga, T.; Sekine, T.; Tanaka, I. Distribution of solute atoms in β-and spinel Si$_{6−z}$Al$_z$O$_z$N$_{8−z}$ by Al K-edge X-ray absorption near-edge structure. *Phys. Rev. B: Condens. Matter Mater. Phys.* **2005**, *71*, 033202.

(11) Brgoch, J.; Gaultois, M. W.; Balasubramanian, M.; Page, K.; Hong, B.-C.; Seshadri, R. Local structure and structural rigidity of the green phosphor β-SiAlON:Eu^{2+}. *Appl. Phys. Lett.* **2014**, *105*, 181904.

(12) Lippmaa, E.; Mägi, M.; Samoson, A.; Tarmak, M.; Engelhardt, G. Investigation of the structure of zeolites by solid-state high-resolution silicon-29 NMR spectroscopy. *J. Am. Chem. Soc.* **1981**, *103*, 4992−4996.

(13) George, N. C.; Pell, A. J.; Dantelle, G.; Page, K.; Llobet, A.; Balasubramanian, M.; Pintacuda, G.; Chmelka, B. F.; Seshadri, R. Local environments of dilute activator ions in the solid-state lighting phosphor Y$_{3−x}$Ce$_x$Al$_5$O$_{12}$. *Chem. Mater.* **2013**, *25*, 3979−3995.

(14) Furdyna, J. K. Diluted magnetic semiconductors. *J. Appl. Phys.* **1988**, *64*, R29−R64.

(15) Hsu, K. F.; Loo, S.; Guo, F.; Chen, W.; Dyck, J. S.; Uher, C.; Hogan, T.; Polychroniadis, E.; Kanatzidis, M. G. Cubic AgPb$_m$SbTe$_{2+m}$: bulk thermoelectric materials with high figure of merit. *Science* **2004**, *303*, 818−821.

(16) Larson, A. C.; Von Dreele, R. B. *GSAS, General Structure Analysis System*; LANSCE: Los Alamos, NM, 1994.

(17) Toby, B. H. EXPGUI, a graphical user interface for GSAS. *J. Appl. Crystallogr.* **2001**, *34*, 210−213.

(18) Momma, K.; Izumi, F. VESTA: a three-dimensional visualization system for electronic and structural analysis. *J. Appl. Crystallogr.* **2008**, *41*, 653−658.

(19) Clark, S. J.; Segall, M. D.; Pickard, C. J.; Hasnip, P. J.; Probert, M. I.; Refson, K.; Payne, M. C. First principles methods using CASTEP. *Z. Kristallogr. - Cryst. Mater.* **2005**, *220*, 567−570.

(20) Pickard, C. J.; Mauri, F. All-electron magnetic response with pseudopotentials: NMR chemical shifts. *Phys. Rev. B: Condens. Matter Mater. Phys.* **2001**, *63*, 245101.

(21) Yates, J. R.; Pickard, C. J.; Mauri, F. Calculation of NMR chemical shifts for extended systems using ultrasoft pseudopotentials. *Phys. Rev. B: Condens. Matter Mater. Phys.* **2007**, *76*, 024401.

(22) Profeta, M.; Mauri, F.; Pickard, C. J. Accurate first principles prediction of ^{17}O NMR parameters in SiO$_2$: assignment of the zeolite ferrierite spectrum. *J. Am. Chem. Soc.* **2003**, *125*, 541−548.

(23) Perdew, J. P.; Burke, K.; Ernzerhof, M. Generalized gradient approximation made simple. *Phys. Rev. Lett.* **1996**, *77*, 3865.

(24) Monkhorst, H. J.; Pack, J. D. Special points for Brillouin-zone integrations. *Phys. Rev. B* **1976**, *13*, 5188.

(25) Bak, M.; Rasmussen, J. T.; Nielsen, N. C. SIMPSON: a general simulation program for solid-state NMR spectroscopy. *J. Magn. Reson.* **2000**, *147*, 296−330.

(26) Zhu, X.; Masubuchi, Y.; Motohashi, T.; Kikkawa, S. The z value dependence of photoluminescence in Eu^{2+}-doped β-SiAlON (Si$_{6−z}$Al$_z$O$_z$N$_{8−z}$) with 1 ≤ z ≤ 4. *J. Alloys Compd.* **2010**, *489*, 157−161.

(27) Takeda, T.; Xie, R.-J.; Hirosaki, N. Local structure analysis in nitride and oxynitride phosphors. *ECS J. Solid State Sci. Technol.* **2013**, *2*, R3132−R3137.

(28) Denault, K. A.; Brgoch, J.; Kloß, S. D.; Gaultois, M. W.; Siewenie, J.; Page, K.; Seshadri, R. Average and Local structure, Debye temperature, and structural rigidity in some oxide compounds related to phosphor hosts. *ACS Appl. Mater. Interfaces* **2015**, *7*, 7264−7272.

(29) Shannon, R.; Prewitt, C. T. Effective ionic radii in oxides and fluorides. *Acta Crystallogr., Sect. B: Struct. Crystallogr. Cryst. Chem.* **1969**, *25*, 925−46.